17th World Conference on Earthquake Engineering, 17WCEE
Sendai, Japan - September 13th to 18th 2020

Testing the quality and performance of various proxies for ground-motion estimates in low-to-moderate seismicity areas: an example from RESIF data (mainland France)

B. Derras[(1)], E.Maufroy[(2)], P-Y.Bard[(3)], C. Beauval[(4)], P.Traversa[(5)]

[(1)] *RISAM laboratory Tlemcen University/Saida University, Algeria, Boumediene.derras@univ-tlemcen.dz*
[(2)] *ISTerre, Grenoble-Alpes University/CNRS/IRD, Grenoble, France, emeline.Maufroy@univ-grenoble-alpes.fr*
[(3)] *ISTerre, Grenoble Alpes University /CNRS/IRD/UGE, Grenoble, France, pierre-yves.bard@univ-grenoble-alpes.fr*
[(4)] *ISTerre, IRD/ Grenoble-Alpes University/CNRS, Grenoble, France, celine.beauval@univ-grenoble-alpes.fr*
[(5)] *EDF-DIPNN Aix-en-Provence University, France, paola.traversa@edf.fr*

Abstract

We take advantage of the RAP-RESIF database (1996 – 2016, http://seismology.resif.fr/), consisting of various ground-motion intensity measures (GMIMs) derived from the French accelerometric and broad-band network recordings, with the associated metadata, to investigate the sensitivity of data-driven ground-motion prediction models (GMPM) to the model parameters. We focus on mainland France. The considered GMIMs are the peak ground acceleration (PGA), the peak ground velocity (PGV), and the pseudo-spectral acceleration PSA(T), while the metadata consist of epicentral distance (Repi), focal depth (Depth), moment magnitude (M_w), local magnitude (M_L) and V_{S30}. The first aim of this study is not yet to derive a new GMPM to be used in PSHA studies (too few data from moderate-to-large magnitude events), but to evaluate the actual performance of the available metadata through an analysis of the aleatory variability obtained for different sets of explanatory variables. The GMPMs are derived with an artificial neural network (ANN) approach including a random-effect procedure. Three different data subsets are considered 1) recordings with only measured V_{S30} estimates, 2) all recordings with all kinds of V_{S30} estimates and 3) recordings with only inferred V_{S30}. The between-event and within-event residuals are calculated at different spectral periods to investigate the relevance and quality of the different explanatory variables. The effects of source and path metadata may be summarized as follows: The joint consideration of M_w and M_L allows some improvements in the short and intermediate period range, the distance dependence should account for both geometrical spreading and anelastic attenuation, the consideration of focal depth brings only marginal improvements in the very short period range. The quality of site metadata impacts not only the within-event variability, but also the between-event one: besides an increased aleatory uncertainty, median predictions may also be significantly affected when V_{S30} values or site class are only inferred. One of the outcome of this preliminary study is therefore to emphasize the need for high-density, high-quality "classical" seismological networks and earthquake bulletins in low-ro-moderate seismicity countries.

Keywords: RAP-RESIF flatfile, Neural network, Ground motion prediction model, France.

2. Introduction

In countries characterized by low-to-moderate seismicity, it is imported models are usually required to import ground motion models determined in other regions of the world to predict ground motions for magnitudes of interest in earthquake engineering ($M_W \geq 5.0$). Indeed, The interevent times of destructive earthquakes are much longer than the lifetime of strong-motion networks. In mainland France, less than 5 earthquakes with $M_W \geq 5.0$ have been recorded since the first strong-motion stations were installed (1996). Nonetheless, the country recently experienced a destructive earthquake at Le Teil in southeastern France (Rénass M_L 5.2, November 11, 2019, epicentral intensity VII-VIII EMS-98, [1]. Such an intensity had not been observed in the French Metropolitan territory since 1967 (Arette earthquake in the Pyrenees).

Until now, probabilistic hazard calculations for metropolitan France have been performed using ground-motion prediction models (GMPM) based on ground-motion data from different databases (Euro-Mediterranean, Western US, global scales or even stochastic data). [2] published a new database, the European Strong Motion (ESM) database, collected by the eponymous service of ORFEUS-EPOS [3], containing mostly data from Italy, Greece and Turkey. French stations represent 5% of stations in the ESM, but only 1% of the ESM recordings come from France (see statistics in [2]).

Using imported models based on data recorded in other regions of the world has some drawbacks. Firstly, the attenuation properties are not necessarily the same from one country to another and may even be drastically different from one region to another (see the recent maps published in France by [4,5]. Secondly, the ground motion recorded at a given station is affected by the site response, which is representative of the local soil characteristics beneath the station, and therefore site-specific. GMPM attempt to compensate for this problem by a good representativeness of soil classes in the data and by the inclusion of site parameters (V_{S30} being the most common). However, these parameters are extremely simple and cannot account for complex site effects that cause high uncertainties, e.g. surface-wave generation in 3D sedimentary basins (such as the French Alpine valleys). GMPM mixing a wide variety of different site responses, they are representative of average site responses within a given soil class and cannot replace the knowledge of the specific response of the soils at a particular site. Finally, it should be noted that the source parameters (magnitude, location, depth) are highly dependent on the networks used to determine them. Variations in these parameters can thus be observed from one institute to another; generally, national services are those providing the most reliable and precise parameters, but regional biases can still appear in their determination. These differences have an impact when exporting GMPM.

In order to better characterize earthquake ground motion on its territory, France has just set up its own national flatfile [6]. This flatfile integrates 20 years (1996-2016) of earthquake records on the metropolitan territory acquired by RESIF stations, including the national strong-motion RAP and broadband RLBP networks [7,8]. This study aims at testing the applicability of artificial neural network methods on this RESIF RAP-RLBP flatfile to derive ground-motion prediction models that are specific to the French territory. The derived models are only valid for the magnitude range represented in the database. We test the sensitivity of this model to different source and site-condition proxies (SCPs), which allows us to assess the relevance of these parameters for France, or the reliability of their determination method.

3. Data sets

The database used in this work [6] consists of 6515 recordings from shallow crustal events (Depth $\leq$ 30 km) located within metropolitan France or in neighboring countries, with magnitudes ranging from M_L 2.4 to 5.6 (Rénass M_L, http://renass.unistra.fr). The dataset usually goes down to M_L 3.5, but it drops to M_L 2.4 in Eastern France (to be compared to M_L 4.0 for the ESM flatfile). An M_W moment magnitude is also associated to each event, most of them have been estimated in the SiHex project [9], a few are obtained by conversion from the M_L Rénass magnitude (conversion equation from [10]). The RESIF RAP-RLBP flatfile includes more than 6500 quality-checked records from 468 earthquakes recorded at 379 stations (including 177 permanent and 202 temporary stations after the experiments by [11,12]). The flatfile contains intensity measures of earthquake ground motions, and the corresponding source and site metadata. All measures underwent an extensive quality-control process, which included manual phase picking, processing scheme

and consistency check by residual analysis (all details provided in [6]. This process is compliant with international standards. In total, nearly 600,000 fields have been filled in.

For this study we have considered only free field recordings, and eliminated all recordings which lack of information either on the instrument installation or on the value of V_{S30}. Applying these criteria reduces the number of available recordings to 2927. This reduced dataset is then divided into two additional subsets according to the quality of V_{S30} information, i.e., measured or inferred, in order to assess its impact on ground motion predictions (aleatory variability analysis and median estimates). The main characteristics of these 3 data sets are listed in Table 1, and their distribution in terms of (M_w, R_{epi}) and (Mw, V_{S30}) is displayed in Fig. 1a ("All V_{S30}" case), 1b ("Measured V_{S30}") and 1c ("Inferred V_{S30}"). One may notice the lack of data at short epicentral distances ($R_{epi} \leq 10$ km for magnitudes up to 3.5-4, and $R_{epi} \leq 50$ km for magnitudes over 4). In the following, these three data sets will be labeled as "DS_i", the index i being ordered as a function of the quality of the site metadata: DS_1 for "Measured V_{S30}", DS_2 for "All V_{S30}", and DS_3 for "Inferred V_{S30}"

Table 1 – Range of magnitude, distance and V_{S30} for the various data set considered in this study

	DS_1 (Measured V_{S30})	**DS_2 (All V_{S30})**	**DS_3 (Inferred V_{S30})**
No. of Earthquakes	336	376	269
No. of recordings	1524	2927	1403
No. of sites	45	78	33
M_w	[2-5.2]	[2-5.2]	[2.3-5.2]
M_L	[2.4-5.6]	[2.4-5.6]	[2.5-5.6]
Depth (km)	[0-30]		
R_{epi} (km)	[0.31-640]	[0.31-663]	[2.31-663]
V_{S30} (m/s)	[171-2090]	[171-3100]	[187-3100]

PGA values range from 10^{-6} m/s^2 to 1 m/s^2. Dependence of PGA with distance is displayed in Fig. 2 for various magnitude intervals. The figure shows clearly the decay of ground motion with distance and with decreasing magnitude, without however any clear trend for a magnitude dependence of the spatial decay rate.

Fig. 3 displays the cumulative distribution functions (CDF) versus M_w, R_{epi}, Depth and V_{S30} for the three data subsets, which allows both to better assess the validity range of the derived GMPMs, and their relative differences. The distributions with respect to (M_w, Depth, R_{epi}) turn out to be rather similar for the three data sets (all V_{S30}, measured V_{S30} and inferred V_{S30}): the amount of data does not influence the (M_w, Depth, R_{epi}) CDF distribution. One can notice however large differences in the V_{S30} distribution: the "inferred V_{S30}" set is strongly biased towards higher V_{S30} (estimated) values, than the "measured V_{S30}" set (which results in an intermediate CDF curve for the "all V_{S30}" case). This trend has already been observed on the NGA-West 2 and RESORCE databases [13]. It is an additional evidence that the semi-qualitative inference of V_{S30} values from geological or slope information is very imprecise and should as much as possible be avoided (as emphasized by [14] comparing measured V_{S30} values with inferred values).

In several cases, only crude indicators of site-condition are available, based on seismic code classification. We therefore also tested the pertinence of this semi-qualitative site condition proxy (SCP) by considering the three EC8 site classes (A: rock, B: soft rock / stiff soil and C: moderately soft soils). Class A corresponds to $V_{S30} > 800$ m/s, class B to $360 < V_{S30} < 800$ m/s, and class C to $180 < V_{S30} < 360$ m/s. Class D (very soft soil) is excluded because it represents less than 2% of the entire data set. The distribution of the three data subsets in terms of EC8 site class are depicted in Fig. 4, and call for two main comments:

i. it emphasizes again the strong, high value bias of "inferred" estimates.

ii. the "measured subset" includes however a large proportion of class A recordings (much larger than in usual strong-motion data bases). This is related with the original choice of accelerometric sites in France, favoring sites with as small as possible site effects in order to better recover source and path effects.

In the following, for sake of simplicity, we will replace R_{epi} by R and Depth by D.

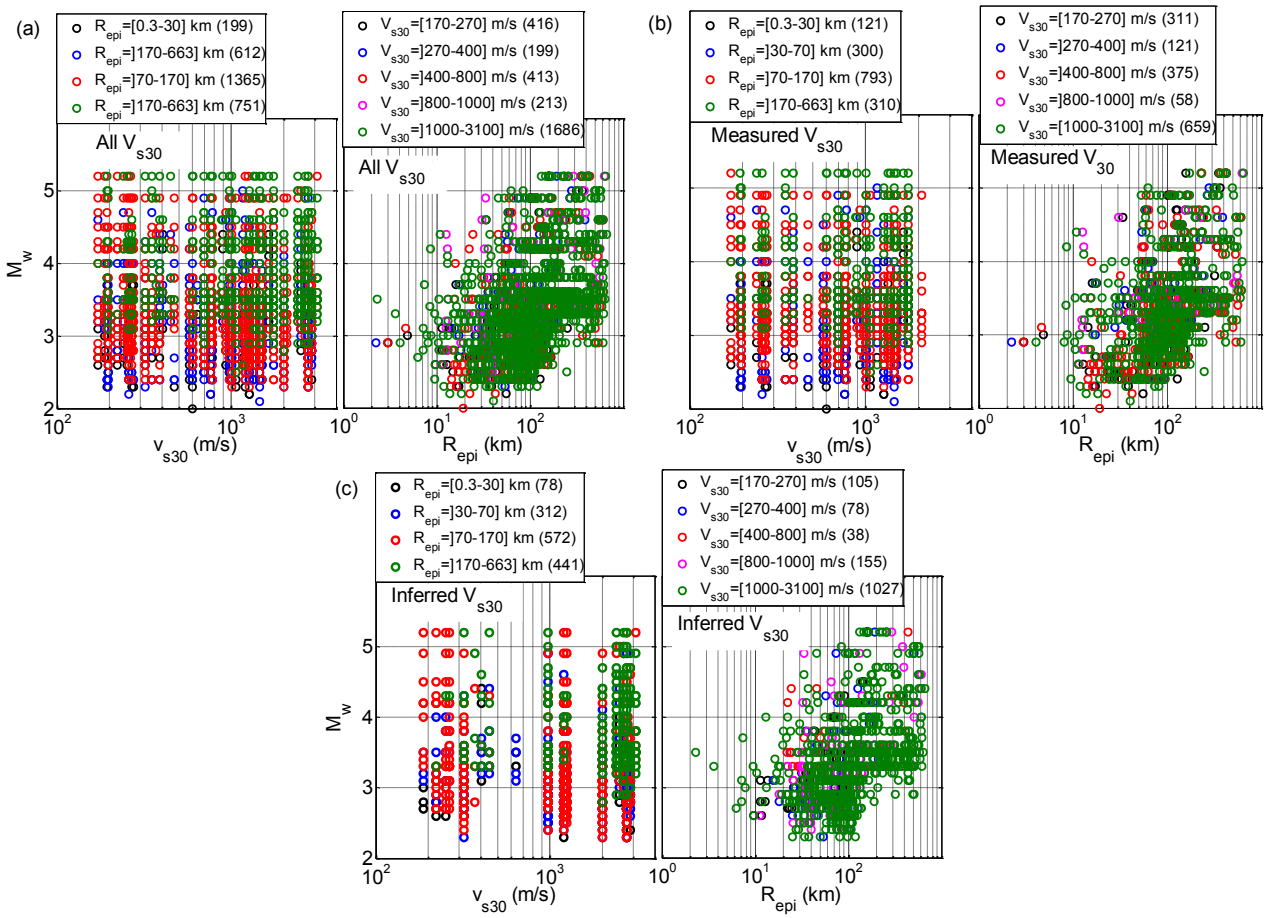

Fig. 1 – Distribution of the three data subsets considered in this study, in terms of magnitude, V_{S30} values and distance R_{epi}. (a) DS_2, all V_{S30}; (b) DS_1, measured V_{S30} subset; (c) DS_3, inferred V_{S30}. Colors correspond to different distance or V_{S30} ranges.

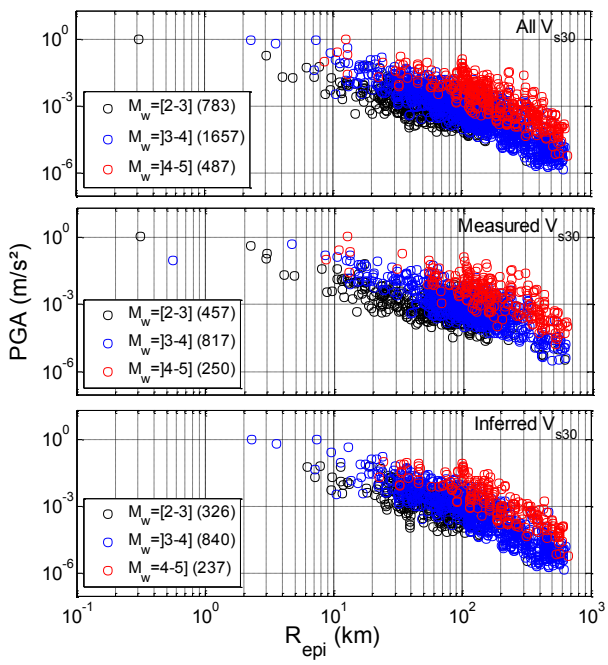

Fig. 2 – Distribution of PGAs with epicentral distance (R_{epi}) for three magnitude intervals. Top: subset "all V_{S30}" case (DS_2); middle: "measured V_{S30}" (DS_1); bottom: "inferred V_{S30}" (DS_3).

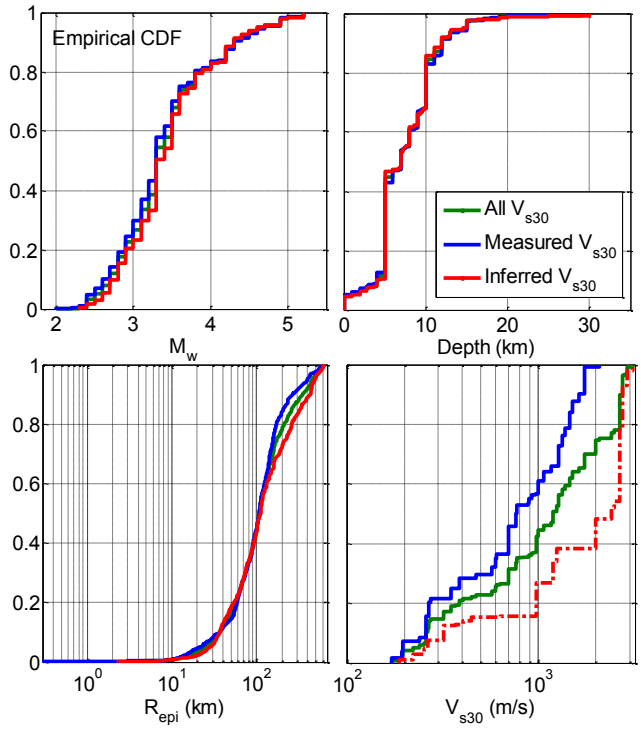

Fig. 3 – Cumulative distribution functions of the four explanatory variables: M_w, Depth, R_{epi} and V_{S30}, for the three subsets "measured V_{S30}" (DS_1, blue), "all V_{S30}" (DS_2, green), and "inferred V_{S30}" (DS_3, red).

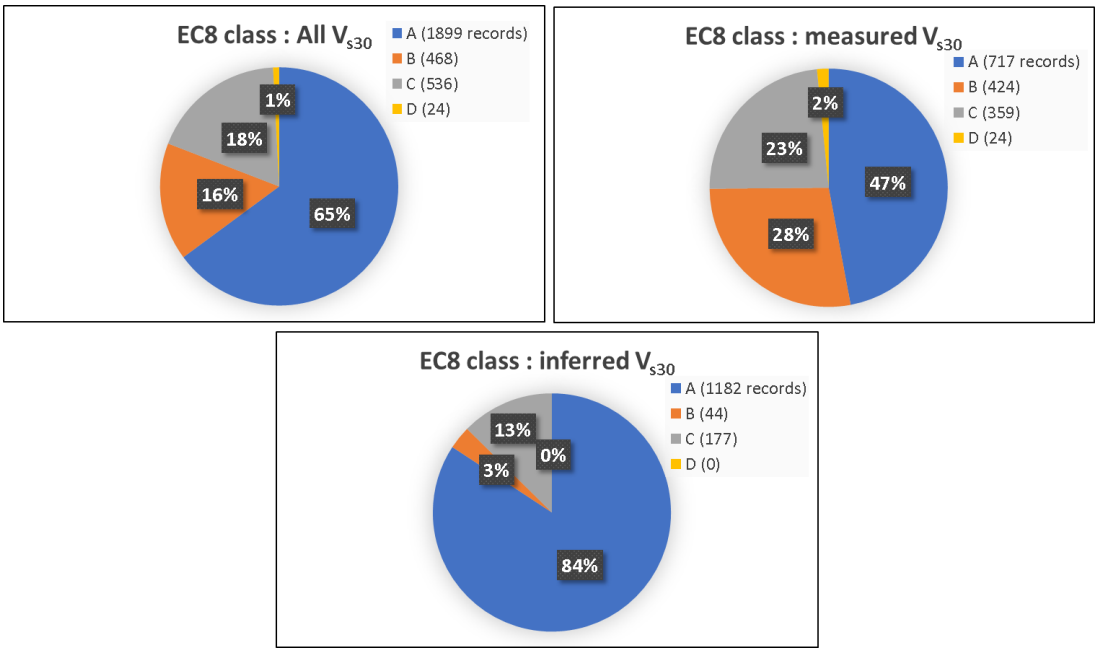

Fig. 4 – Distribution of the three considered data subsets (all, measured and inferred V_{S30}) in terms of EC8 site classes (A-B-C).

4. Methodology

The random-effects procedure proposed by [15] and adapted for the neural network approach by [16] is adopted to obtain the GMPMs. These models are used to investigate the effects of the choice of the explanatory variables on 1) the level of ground-motion aleatory variability and 2) the median ground-motion

models. This resulted in a two-phase building process, starting with a fixed-effects model as step 1 and a random-effect model as step 2.

The first step is to establish the fixed models. The explanatory parameters are M_W and/or M_L to characterize the source size, R_{epi} and Depth to characterize the path characteristics, and the information based on V_{S30} to describe the site conditions. In the fixed-model, to the contrary of most GMPMs, both M_W and M_L are used, as they are supposed to impact differently the low- and high-frequency motion.

The predicted ground motions are the geometric mean horizontal component of PGA, PGV, and 5%-damped PSA at 20 periods from 0.02 s to 10 s. We do not include equations for peak ground displacement (PGD), which we consider to be too sensitive to the low-pass filters used in the data processing, and which vary a lot from one recording to another [13].

A multilayer perceptron ANN architecture is used. The structure of the ANN is displayed in Fig. 5. The input and output layers contain the input and output parameters and are linked through one single hidden layer consisting of three neurons. The type of activation function between input and hidden layers, and between hidden and output layers, has been adopted after several tests [17]. It resulted in the choice of a "tangent sigmoid" type for the hidden layer and a "linear" one for the output layer. The quasi-Newton backpropagation technique has been applied for the training phase [18]. To avoid over-fitting problems, we chose an adequate regularization method as developed by [19]. In Fig. 5, the symbols W and b represent the synaptic weights and bias with subscripts representing the corresponding neurons between two layers.

Several ANN models were built, differing by the data set and the SCP used in the input layers. For the three data sets (All V_{S30}, measured V_{S30}, inferred V_{S30}) the source and path are described by M_w, M_L, focal depth D and the epicentral distance R_{epi}. A first ANN model was considered with only those four input parameters (M_w, M_L, Depth and R_{epi}) without any SCP, in order to set the reference for quantifying the gains brought by the consideration of the various site proxies. The proxies describing the site conditions are the site classes derived from the V_{S30} values (EC8 class A, B and C), or the V_{S30} value (inferred or measured).

In the second step, a procedure similar to the random-effects approach was used to provide the between- and within-event sigma, as described in Derras et al. (2014). The performance of the ANN is measured by the total standard-deviation σ, which is decomposed into the between-event (τ) and within-event (ϕ) variabilities [20], according to the following Eq. (1) for each period T:

$$\sigma(T) = \sqrt{\tau^2(T) + \phi^2(T)} \tag{1}$$

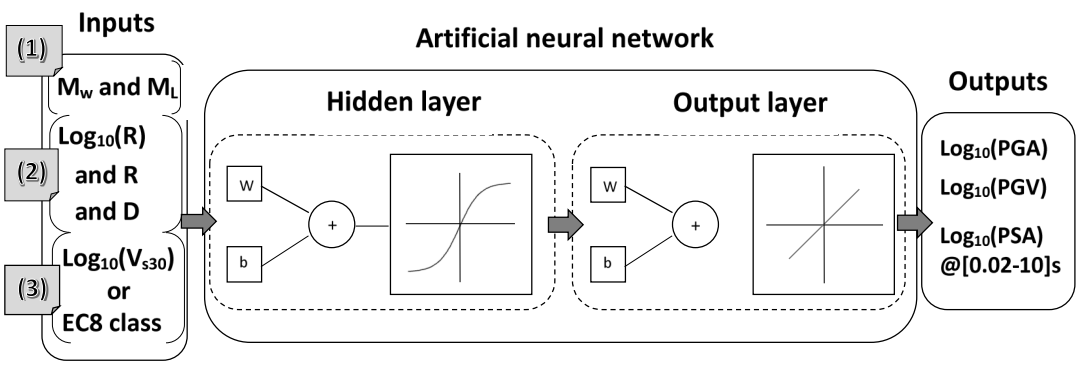

Fig. 5 – Structure of the neural networks considered for the prediction of PGA, PGV and PSA [0.01 to 10 s]. W is the synaptic weight and is b the bias. (1) deals with the source effect parameters, (2) with the path effect and (3) represent SCPs.

5. Performance of the various proxies on ground-motion aleatory variability

5.1 Assessment of ground-motion aleatory variability

In this section, we compare the various models derived for each data set and analyze how the various source, path parameters and SCPs reduce the ground motion variability. The best way to measure the efficiency of

the given path parameters and SCPs is not to look at the absolute levels of {τ, ϕ, σ}, but to observe how they contribute to the variance reduction coefficient "R" as a function of the oscillator period T. The R is defined in Eq. (2).

$$\begin{cases} R_{\sigma}(T) = (1 - \dfrac{\sigma^2(T)_{ANN(DS_i,\ \text{Parameters set})}}{\sigma^2(T)_{ANN(DS_i,\ \text{reference parameters set})}}) \times 100; \\ R_{\tau}(T) = (1 - \dfrac{\tau^2(T)_{ANN(DS_i,\ \text{Parameters set})}}{\tau^2(T)_{ANN(DS_i,\ \text{reference parameters set})}}) \times 100;\ (\%) \\ R_{\phi}(T) = (1 - \dfrac{\phi^2(T)_{ANN(DS_i,\ \text{Parameters set})}}{\phi^2(T)_{ANN(DS_i,\ \text{reference parameters set})}}) \times 100; \end{cases} \quad (2)$$

Where *ANN(DS_i, parameters set)* and *ANN(DS_i, reference parameters set)* represent the artificial Neural Network model in which we use one of the three data sets (DS_1 : measured, DS_2 : all or DS_3 : inferred V_{S30}). Various ANN models are derived for each data set, considering various combinations of source and path parameters, either with or without SCP (V_{S30} or EC8 class). In the two following sections we will represent the different developed ANN model (GMPMs).

5.2 Source and path parameters test procedure without site-condition proxies

Ground motions have to be predicted for target sites which may have different site condition descriptions. We first consider the case where no information on V_{S30} or class of V_{s30} are available, and call it "*without(SCP)*". We then developed five models for the largest dataset (DS_2)

1. The base model used as a reference considers only M_w and $\log_{10}(R_{epi})$; it is labeled *ANN(DS_2, M_w+log_{10}(R), without(SCP))*.
2. To investigate the interest of adding another magnitude, we compare the base model with another model *ANN(DS_2, M_w+log_{10}(R)+$\boldsymbol{M_L}$, without(SCP))*.
3. In order to investigate the potential contribution of anelastic attenuation, we consider both log10(R) and R in the set of explanatory variables, *ANN(DS_2, M_w+log_{10}(R)+**R**, without(SCP))*, and compare it with the base model.
4. The improvement brought by the consideration of focal depth is analyzed by considering a fourth model *ANN(DS_2, M_w+log_{10}(R)+**D**, without(SCP))*.
5. Finally, to get an idea of the best possible variability reduction without considering any SCP, a final reference model is considered considering all 5 source and propagation proxies: *ANN(DS_2, Mw+log_{10}(R)+**R**+$\boldsymbol{M_L}$+**D**, without(SCP))*.

This set of five models thus allowed to assess the pertinence of source and path parameters (without any account of site conditions through any SCPs). The variance reduction coefficients R are presented in the Fig. 6. The performances are measured on the within-events, between-events and total standard deviation (Eq.1). A quick reading of this Figure shows that:

i. Whatever the considered models, the largest contribution to the variance reduction is provided, as expected, by the between-event term, τ.
ii. The simultaneous consideration of both R and $\log_{10}$(R) leads to the largest variance reduction (compared with M_L and D), with a maximum efficiency at intermediate periods (around 0.3 – 0.6 s)
iii. Considering the local magnitude in addition to M_w slightly reduces the aleatory variability in the short period range (as expected since M_L is measured at shorter periods than M_W), and mostly from the between-event component
iv. Considering the focal depth leads to tiny improvements, and only at very short periods (T≤ 0.1 s). One should note however that the reliability of hypocentral depth values is limited, especially for small magnitude events. The result could be different if considering more precise depth estimates (see for instance [21]).

Therefore, in the following section, we will base our analysis of site condition proxies performance on the "best" source and path models, i.e., those accounting for the 5 parameters M_W, M_L, $\log_{10}(R)$, R and D.

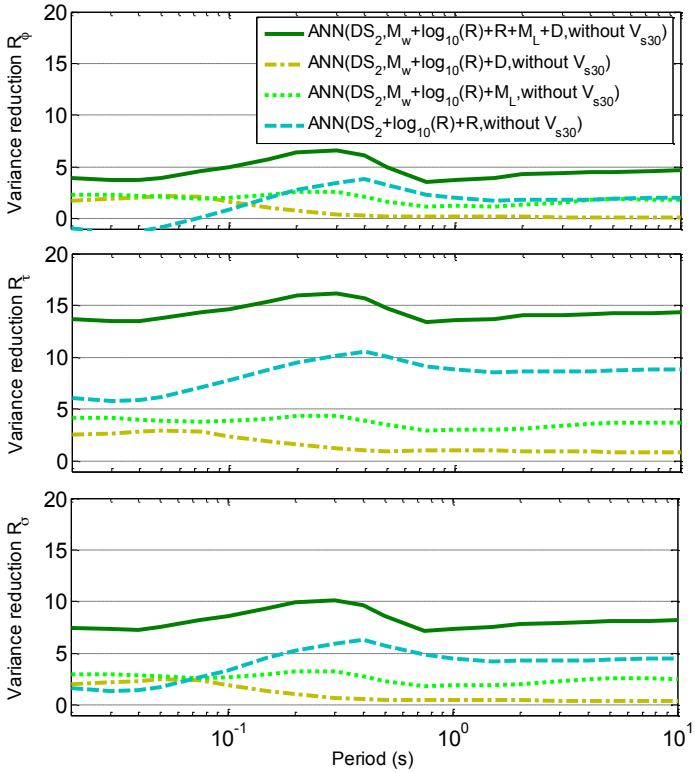

Fig. 6 – . Quantifying the performance of the various source and path parameters considering the largest data set DS_2. Variance reduction coefficient as a function of oscillator period for the within-event (top), between-event (middle) and total variabilities (bottom).

5.3 Site-condition proxies test

In this second test, we considered the three data sets DS_i (i=1, 2 or 3), and for each of them we derived two models with the two different SCPs V_{S30} and EC8 class, which are compared with the corresponding "without SCP" reference model, consisting in each case of the "best" model using the five source and path parameters (M_w, M_L, $\log_{10}(R)$, R, D). The reference models are thus *ANN (DS_i, $Mw+\log_{10}(R)+R+M_L+D$, without(SCP)), and the two* other models for each data set are:

1. one model using the continuous V_{S30} value as an input, named *ANN(DS_i, $Mw+\log_{10}(R)+$**$R+M_L+D$**, **$\log_{10}(V_{S30})$**)*.
2. one model using the EC8 site class information, named *ANN(DS_i, $Mw+\log_{10}(R)+$**$R+M_L+D$**, **EC8**)*.

The variance reduction coefficients defined in Eq. (2) are displayed as a function of the oscillator period in Fig. 7, for each data set. From these results, we can draw the following comments and conclusions:

i. The largest reductions obtained with site information logically correspond to the data set 1 with Measured V_{S30}, whatever the considered SCP (V_{S30} or EC8 class). In the first case, the reduction exhibits a clear dependence on period with a limited impact at short period (minimum around 20 % for T= 0.075 s for the total variability), and the largest one in the intermediate period range (maximum around 40% for T between 0.5 and 1.0 s).
ii. The smallest reductions correspond to data set 3 including only inferred V_{S30}, and especially when considering only the EC8 site class. In that latter case, the reduction lies in the range [3.5 - 7.0] %, without any significant period dependence
iii. For the data set DS_2 (mixing all kind of V_{S30} information), the SCP performances are intermediate, reaching at most 25%, with only a weak period dependence

iv. The largest reduction for the DS_2 data set occurs on the between-event component. This is somehow surprising, but may be understood when considering that a better accounting of site effects allows to better separate the source and path contributions from the site terms, thus in turn to better constrain the path and source terms, and therefore to significantly reduce the between-event variability. Actually, the average value of the between-event variability turns out to be as large as 0.3 ($\log_{10}$) for DS_3 (with or without a site proxy), while it drops down to 0.15 for DS_1 (and about 0.25 for DS_2).

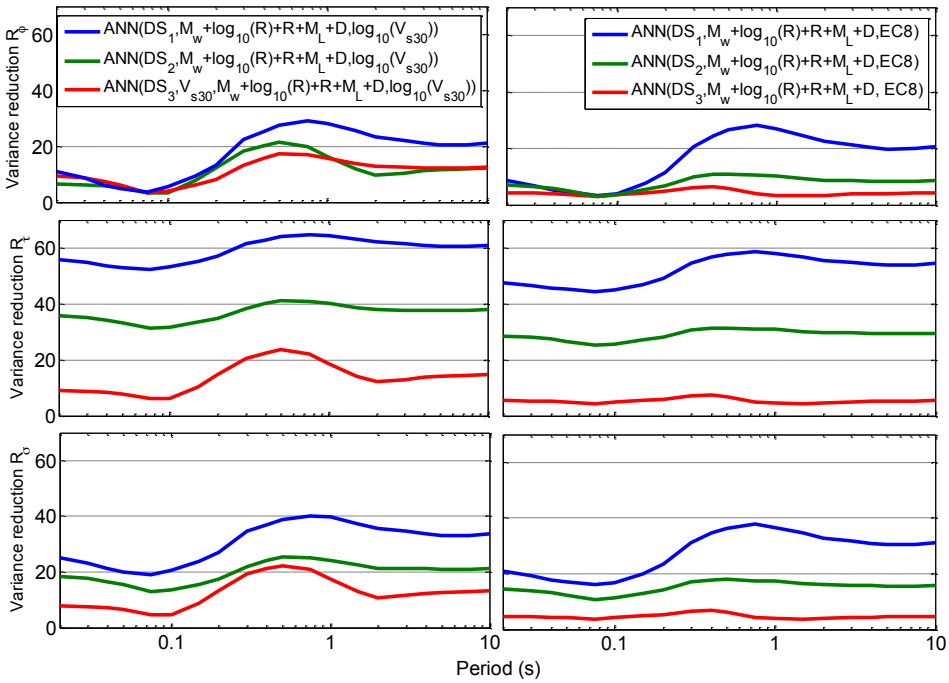

Fig. 7 – Improvement brought by the consideration of SCPs (V_{S30} –left - and EC8 class - right) for the three data sets "All V_{S30}" in green, ("measured V_{S30}" in blue and "inferred V_{S30}" in red). Variance reduction for the within-event (top), between-event (middle), and total aleatory variability (bottom).

The effects of the input parameters on the aleatory variability can be analyzed by a look at the synaptic weights P corresponding to the six input parameters (M, R, D and V_{s30}). These P parameters are a measure of the relative importance of each individual predictor variable. They have been computed according to the procedure detailed in [16]. The three data sets have been considered (DS_1, DS_2 and DS_3). The most efficient parameter in reducing the variance of response spectra is the epicentral distance (P from 40 to 47 %), followed directly by the earthquake magnitude (around 30–34% when both M_W and M_L are considered). The P associated to the V_{s30} range from 13% to 18%: The largest SCP weights correspond to measured V_{S30} and the smallest correspond to Inferred V_{S30}. These P(V_{S30}) values are larger than for NGA-West 2 [13] and comparable with those found for KiK-Net [22].

Table 2 – Sensitivity of ground motion models to magnitude, distance and site parameters (V_{s30}), as expressed through the total percentages of synaptic weight (P, %) corresponding to each input parameter

ANN models	P (%)					
	$Log_{10}(R)$	R	D	M_w	M_L	V_{S30}
ANN(DS_1,Mw+log10(R)+R+M_L+D,$\log_{10}(V_{S30})$)	26	14	8	18	16	**18**
	48			**34**		
ANN(DS_2,Mw+log10(R)+R+M_L+D,$\log_{10}(V_{S30})$)	32	14	7	16	14	**17**
	53			**30**		
ANN(DS_3,Mw+log10(R)+R+M_L+D,$\log_{10}(V_{S30})$)	25	22	6	17	17	**13**
	53			**34**		

6. Aleatory variability: Comparison with other ANN-datasets models

In this section, we shortly compare the variability levels obtained for the RESIF-RAP database, with those derived from databases including larger magnitude data sets, with the same ANN approach: RESORCE [16], NGA-West 2 [13] and a KiK-Net subset [22]. Table 3 describes the content of these 4 databases. As expected, they differ on the magnitude range as well as on the distance definition (R_{JB} Joyner-Boore distance can be estimated for moderate-to-large magnitude events but is comparable to R_{epi} for small events). The RESIF database is the one that includes the lowest magnitudes. The only model where the focal-mechanisms have been used is [16], based on RESORCE database. In the four models, measured V_{S30} have been chosen.

The aleatory variability for the best models derived from these four databases is displayed in Fig. 8. The RESIF database led to the larger variability, especially in the intermediate to long period range. We think that the main cause for this is the low magnitude range, which implies larger uncertainties in the magnitude and location estimates. Further investigations will be carried out in a future step.

Table 3 – Description of the dataset used to derive four ground-motion prediction models with an ANN approach: RESORCE, KiK-Net, NGA-West 2 and RESIF databases

Data set	Distance range (km)	Focal depth range (Km)	Magnitude type and rang	Focal-mechanism	Measured V_{S30} range (m/s)
RESIF with DS_1 [This study]	R_{epi}=[0.31-640]	0-30	M_w=[2.0-5.2] M_L=[2.4-5.6]	-	171-2090
RESORCE [16]	R_{JB}=[5-200]	0-25	M_w=[4.0-7.0]	N, R, SS	200-800
KiK-Net [22]	R_{JB}=[3.65-440.6]	0-30	M_w=[3.7-6.9]	-	153-1433
NGAWest 2 [13]	R_{JB}=[10^{-3}-1533]	-	M_w=[3.0-7.9]	-	89-2100

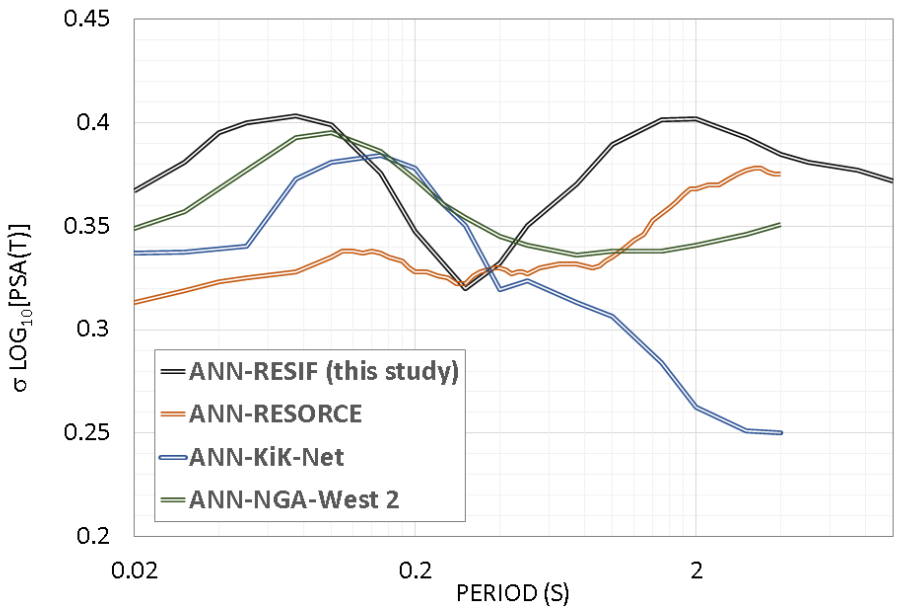

Fig. 8 – Comparison of the total (σ) standard deviations.

7. Conclusion

This preliminary analysis of the RAP-RESIF data base allows to draw a few preliminary conclusions regarding the event and site metadata that should be gathered in view of deriving GMPMs which could be used for seismic hazard assessment in moderate seismicity countries.

- Regarding the source parameters, the joint consideration of several magnitude estimates (here M_w and M_L) does help in reducing the aleatory uncertainty, especially in the high frequency range. Such a double

event size characterization might be particularly interesting for low magnitude events, it could also be a direction for further investigations for "classical" GMPMs over larger magnitude data sets, as the two kinds of magnitude control different frequency ranges, and could be a simple alternative for the consideration of the difficult to measure stress-drop parameter.

- Regarding path parameters, this ANN study emphasizes a result which is already well known for classical GMPMs, i.e., the joint use of log(R) and R as input allows a better accounting of geometrical spreading and anelastic damping. Meanwhile the information about hypocentral depth provides only a very marginal improvement, which could be explained by the large associated uncertainty
- Regarding the site condition proxies, our results confirm once again the significant improvements brought by site-specific velocity measurements are very significant; a side, interesting result, is the porosity between between- and within-event uncertainties when the site conditions are considered through very fuzzy estimates, which in turn indicate the impact of SCP on the estimation of path and/or source terms.
- In addition, the development of GMPMs valid for low magnitude events (which is needed for instance for deriving site-specific residuals in low-to-moderate seismicity countries) requires a specific attention to the source metadata, and therefore the maintenance of high-density seismological networks and the careful daily determination of magnitudes and hypocentral locations.

This preliminary analysis will be complemented by further investigations aiming first at assessing the robustness of the above mentioned results and the selection of "optimal" input parameters, and the possibility of regional changes in the spatial decay, and in a second step a combination with other, larger-magnitude European data (i.e., the ESM data base) to derive FGMPMs which could be directly used for hazard assessment studies in mainland France.

8. Acknowledgments

The authors would like to thank the participants of the RESIF-RAP program for providing high quality data and stimulating ideas. We acknowledge the support from the DEVMOD project “Développement de modèles de prédiction des mouvements sismiques dirigés par les données et implications pour les estimations d'aléa sismique: application aux données RESIF RAP et RLBP, et RESORCE”. The authors are grateful also to Algerian Directorate General for Science Research and Technological development (DGRST).

9. Data and resources

The datasets used in this article have been collected by ‘RESIF SEISMIC DATA PORTAL’ http://seismology.resif.fr.

10. References

[1] Schlupp A, Sira C, Maufroy E, Provost L, Dretzen R, Bertrand E, Beck E, Schaming M (2020): EMS98 intensity estimation of the shallow Le Teil earthquake, M_L 5.2, by Macroseismic Response Group GIM. *EGU General Assembly,* Vienna, Austria.

[2] Lanzano G, Sgobba S, Luzi L, Puglia R, Pacor F, Felicetta C, D’Amico M, Cotton F, Bindi D (2019): The pan-European Engineering Strong Motion (ESM) flatfile: compilation criteria and data statistics. *Bulletin of Earthquake Engineering*, **17**(2), 561-582.

[3] Luzi L, Puglia R, Russo E, D’Amico M, Felicetta C, Pacor F, Lanzano G, Ceken U, Clinton J, Costa G, Duni L, Farzanegan E, Guéguen P, Ionescu C, Kalogeras I, Özener H, Pesaresi D, Sleeman R, Strollo A, Zare M (2016): The Engineering Strong-Motion database: a platform to access pan-European accelerometric data. *Seismological Research Letters*, **87**(4), 987-997.

[4] Mayor J, Bora S.S, Cotton F (2018a): Capturing regional variations of hard-rock κ_0 from coda analysis. *Bulletin of the Seismological Society of America*, **108**(1), 399-408.

[5] Mayor J, Traversa P, Calvet M, Margerin L (2018b): Tomography of crustal seismic attenuation in Metropolitan France: implications for seismicity analysis. *Bulletin of Earthquake Engineering*, **16**(6), 2195-2210.

[6] Traversa P, Maufroy E, Hollender F, Perron V, Bremaud V, Shible H, Drouet S, Guéguen P, Langlais M, Wolyniec D, Péquegnat C, Douste-Bacque I (2020): RESIF RAP and RLBP dataset of earthquake ground motion in mainland France. In revision *for Seismological Research Letters*.

[7] RESIF (1995a). RESIF-RAP French Accelerometric Network. *RESIF - Réseau Sismologique et géodésique Français*. *Doi: 10.15778/RESIF.RA*.

[8] RESIF (1995b). RESIF-RLBP French Broad-band Network, RESIF-RAP strong motion network and other seismic stations in metropolitan France. *RESIF - Réseau Sismologique et géodésique Français*. *Doi: 10.15778/RESIF.FR*.

[9] Cara M, Cansi Y, Schlupp A et al (2014): Si-Hex: a new catalogue of instrumental seismicity for metropolitan France. *bulletin de la société géologique de france* **186**(1),3-19.

[10] Grünthal G, Stromeyer D, Wahlström R (2009): Harmonization check of Mw within the central, northern, and northwestern European earthquake catalogue (CENEC). *Journal of Seismology*. **13**(4), 613-632.

[11] Chevrot S, Sylvander M (2017): Seismic network X7: PYROPE PYRenean Observational Portable Experiment (RESIF-SISMOB), *RESIF-Réseau sismologique et géodésique français*. Doi: 10.15778/resif.x72010.

[12] Zhao L, Paul A, Solarino S, RESIF (2016): *Seismic network YP: CIFALPS temporary* experiment (China-Italy-France Alps seismic transect). *RESIF-Réseau Sismologique et géodésique Français*. doi.org/10.15778/RESIF.YP2012.

[13] Derras B, Bard P-Y, Cotton F, (2016): Site-conditions proxies, ground-motion variability and data-driven GMPEs insights from NGA-West 2 and RESORCE datasets. *Earthquake Spectra* **32**(4), 2027–2056.

[14] Hollender F, Cornou C, Dechamp A, Oghalaei K, Renalier F, Maufroy E, Burnouf C, Thomassin T, Wathelet M, Bard P.-Y, Boutin V, Desbordes C, Douste-Bacque I, Foundotos L, Guyonnet-Benaize C, Perron V, Régnier J, Roulle A, Langlais, Sicilia D (2018). Characterization of site conditions (soil class, V_{S30}, velocity profiles) for 33 stations from the French permanent accelerometric network (RAP) using surface wave methods. *Bulletin of Earthquake Engineering*, **16** (6), 2337-2365.

[15] Abrahamson N. A, Youngs R.R, (1992): A stable algorithm for regression analyses using the random-effects model, *Bulletin of the Seismological Society of America,* **82**(1), 505–510.

[16] Derras B, Bard P-Y, Cotton F, (2014a): Towards fully data-driven ground-motion prediction models for Europe, *Bulletin of Earthquake Engineering* **12**(1), 495-516.

[17] Derras B, (2014b): Peak Ground Acceleration Prediction Using Artificial Neural Networks Approach: Application to the Kik-Net Data. *International Journal of Earthquake Engineering and Hazard Mitigation*. **2**(4). doi.org/10.15866/irehm.v2i4.7121.

[18] Shanno D.F, Kettler P.C (1970): Optimal Conditioning of Quasi-Newton Methods. *Math. Comp* **24**(11), 657-664.

[19] Derras B, Bard P-Y, Cotton F, Bekkouche A (2012): Adapting the neural network approach to PGA prediction: an example based on the KiK-net data, *Bulletin of the Seismological Society of America*. **102**(4), 1446–1461.

[20] Al Atik L, Abrahamson N, Bommer J. J, Scherbaum F, Cotton, F, Kuehn N (2010): The variability of ground-motions prediction models and its components, *Seismolorical Research. Letters* **81**(5), 794–801.

[21] Maufroy E, Chaljub E, Hollender F, Bard P.-Y, Kristek J, Moczo P, De Martin F, Theodoulidis N, Manakou M, Guyonnet-Benaize C, Hollard N, Pitilakis K (2016): 3D Numerical simulation and ground motion prediction: Verification, validation and beyond - lessons from the E2VP project. *Soil Dynamics and Earthquake Engineering*. **91**, 53–71.

[22] Derras B, Bard P.-Y, Cotton F, (2017): V_{S30}, slope, H_{800} and f_0: Performance of various site-condition proxies in reducing ground-motion aleatory variability and predicting non-linear site response, *Earth, Planets and Space*, **69**(133).